Insights of Shadow Trapping States and Intramolecular Charge Transfer on Simultaneous Redshift and Efficiency Enhancement of Electrochemiluminescence in Carbon Dots

Erli Yang[a], Hong Yang[a], Zhenqiang Ning[a], Yanfeng Fang[a], Mengyuan Chen[a], Yongjun Zheng[a], Guoqiu Wu[abc], Yuanjian Zhang[a] and Yanfei Shen[abc]∗

[a] *Medical School, School of Chemistry and Chemical Engineering, Southeast University, Nanjing 210009, China.*

[b] *Center of Clinical Laboratory Medicine, Zhongda Hospital, Southeast University, Nanjing 210009, China.*

[c] *Jiangsu Provincial Key Laboratory of Critical Care Medicine, Southeast University, Nanjing 210009, China.*

Email: Yanfei.Shen@seu.edu.cn

Abstract

While highly efficient electrochemiluminescence (ECL) emitters with finely tunable emission wavelengths are crucial for practical applications, the simultaneous modulation of ECL efficiency and emission wavelength, along with the deep understanding of the mechanism in the molecular level, remain elusive. Herein, we reported carbon dots (CDs) with both fine-tuned ECL efficiency and emission wavelength were achieved by phosphorus (P) doping, e.g., the ECL emission was finely tuned from 425 nm to 645 nm, and the efficiency (relative to the $Ru(bpy)_3^{2+}/K_2S_2O_8$ system) was promoted from 10.6% to 57.4%. Experimental and theoretical studies revealed the P dopants in the form of P-C and P-O groups not only imported shadow trapping states but also promoted a significant intramolecular charge transfer (ICT), which jointly induced the redshift and boosted the ECL performance of CDs. This work would provide a clue for the rational design of CDs to tune the ECL properties for advanced biomedical applications finely.

Introduction

Electrochemiluminescence (ECL) is a light-emitting process excited through electrochemical reactions, showing remarkable merits of high sensitivity, low background, quick response, ease of operation, and low cost of equipment.[1-6] Recently, multicolor ECL has attracted considerable attention for ECL-based biomedical applications ranging from multiplex bioassay to bioimaging, raising an increasing demand for exploiting luminophores with tunable emission wavelength.[7-11] However, the development of multicolor ECL-based biomedical applications was somewhat restricted. In this context, it has been reported that multicolor ECL could be realized by combining or modifying ruthenium (II) and iridium (III) complexes.[12-14] Although organic molecules hold great potential for multicolor ECL due to their structural versatility and ease of modulating the electronic and optical properties, most of these studies have been performed in organic media. Inorganic nanocrystals have also been employed for this purpose, mainly using Pb and Cd-based quantum dots (QDs).[15-19] However, it is still challenging to develop highly efficient ECL luminophores with tunable wavelength, excellent water solubility, and biocompatibility.

Carbon dots (CDs) have been emerged as potential emitting materials for ECL due to their merits of ease of surface functionalization, high water solubility, favorable biocompatibility, and excellent environmental friendliness.[20-25] It has been generally believed that the ECL emission of CDs is mainly dominated by surface energy levels and surface chemistry, while photoluminescence (PL) is primarily produced from the core.[26] Numerous efforts have been devoted to the ECL enhancement of CDs by heteroatom doping,[27-29] hybridization with dye[22] or graphene[30], and the oxidation of CDs surface.[31, 32] However, despite these great successes in ECL of CDs, the simultaneous modulation of ECL efficiency and emission wavelength in a wide range, along with an understanding of the mechanism in the molecular level, has been rarely reported.
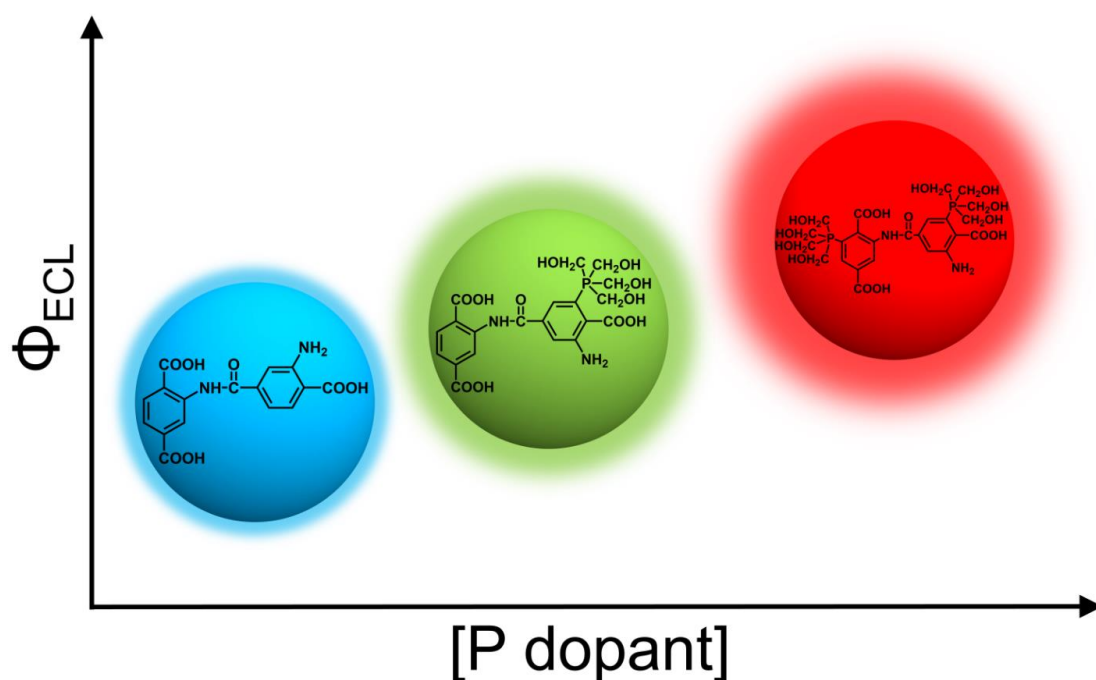
Figure 1. Modulation of ECL wavelength and efficiency of CDs by P-doping in aqueous solution.

Herein, we report a facile way to modulate the ECL emission of CDs in an aqueous solution by phosphorus (P) doping (Figure 1). Thanks to the high electron-donating property of the P dopant, the surface state, band gap, and electrochemical activity of CDs were significantly altered. As a result, the ECL emission was finely tuned from 425 nm to 645 nm solely by adjusting the concentration of P dopants; meanwhile, the ECL efficiency (relative to that of the $Ru(bpy)_3^{2+}/K_2S_2O_8$ system) of CDs was promoted from 10.6% to 57.4%. This unusual fine regulation of both ECL emission wavelength and efficiency was further explored by the kinetics studies and theoretical calculation. It was disclosed that P dopants in the form of P-C and P-O groups not only imported shadow trapping states as previously reported[22, 33] but also promoted intramolecular charge transfer (ICT) in ECL. This work would provide new insight into the correlation between the elemental doping and ECL of nanocarbon, and open a new avenue for the desirable design of nanocarbon towards given applications.
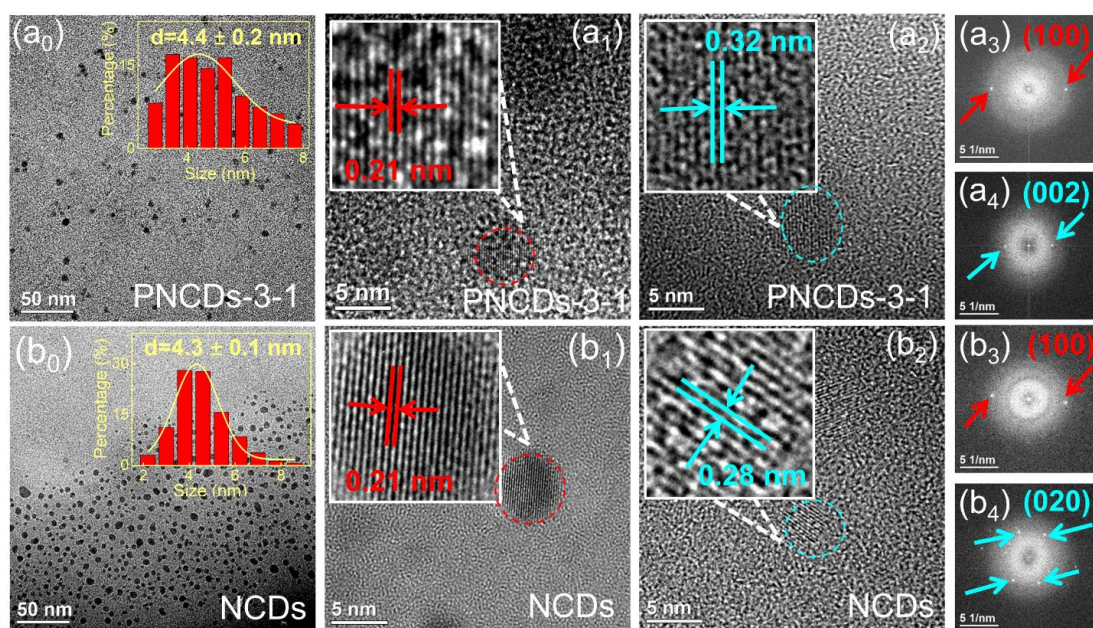
Results and Discussion

Figure 2. TEM images of PNCDs-3-1 (a_0) and NCDs (b_0) with the size distribution in the inset, HRTEM images of PNCDs-3-1 (a_1 and a_2) and NCDs (b_1 and b_2) with insets of zoomed-in images showing crystalline lattice fringes, and FFT patterns of PNCDs-3-1 (a_3 and a_4) and NCDs (b_3 and b_4).

Since surface functional groups play a critical role in ECL generation, 2-aminoterephthalic acid (ATA) was selected as a precursor for synthesizing CDs with ECL properties due to its amine and carboxyl groups (the as-obtained CDs were denoted as NCDs).[33, 34] Given the sizeable atomic radius and high electron-donating ability of P, bis[tetrakis(hydroxymethyl)phosphonium] sulfate solution (THPS) was chosen as an additional precursor for P source to produce P-doped CDs (PNCDs). By adjusting the molar ratio of THPS (m) and ATA (n), different PNCDs-m-n were obtained (Table S1). The transmission electron microscopy (TEM) images of PNCDs and NCDs revealed homogeneous and monodispersed nanoparticles with an average size of 3-8 nm (Figure 2 and Figure S1). The high-resolution TEM (HRTEM) images and corresponding fast Fourier transform (FFT) patterns of PNCDs, and NCDs (Figure 2 and Figure S1) demonstrated a structure with three main types of lattice fringe distance of 0.21 nm, 0.28 nm, and 0.32 nm, corresponding to the (100), (020) and (002) planes of graphitic carbon, respectively.[35-38] Interestingly, compared to the NCDs, the X-ray diffraction (XRD) patterns of PNCDs showed an obviously broadened peak (Figure S2), attributing to the defects in the crystal structure, which was also

revealed by the increased ratio of the disordered D band and crystalline G band (D/G) in the Raman spectra (Figure S3).
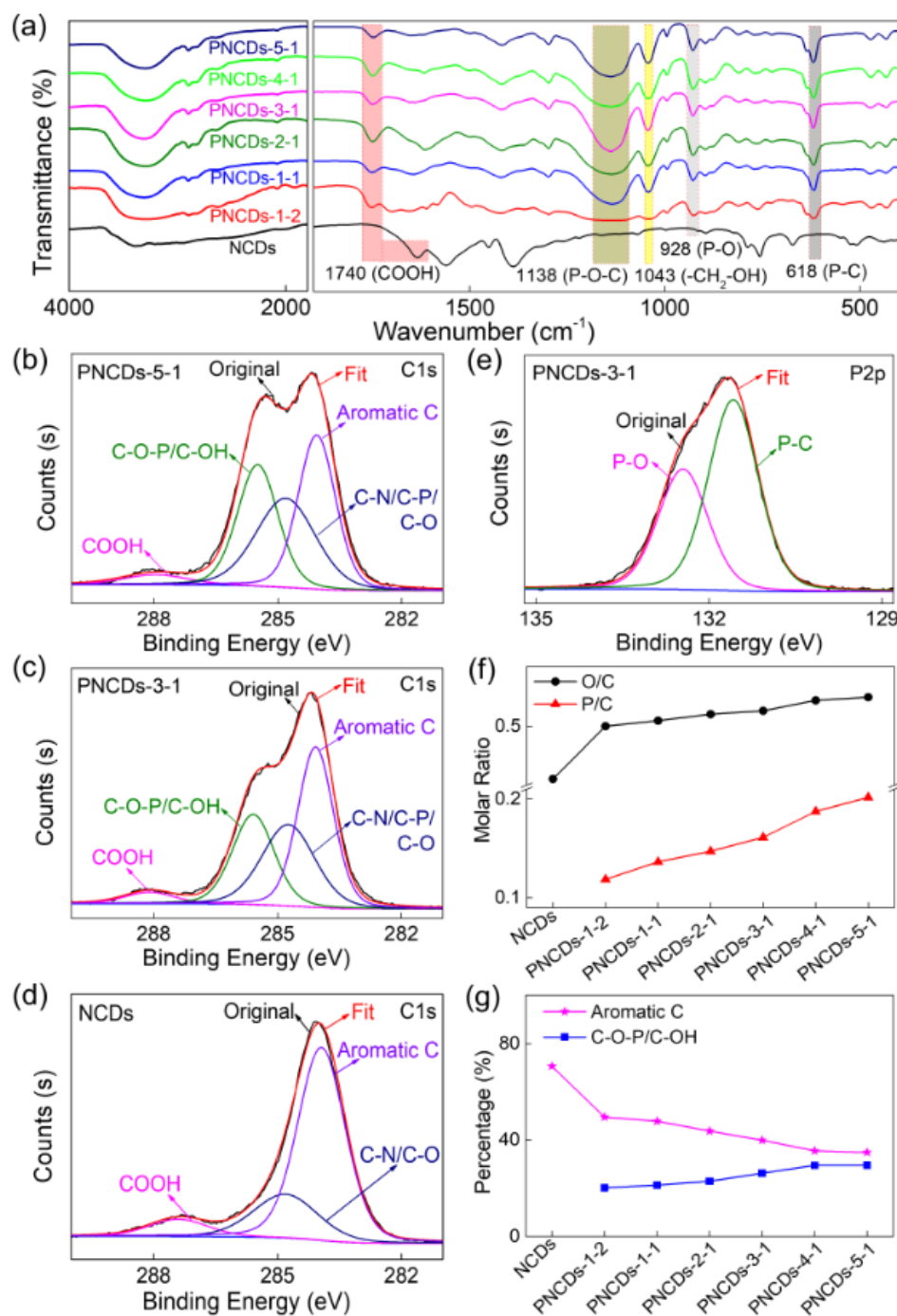

Figure 3. (a) FTIR spectra of NCDs and PNCDs-m-n. The C1s XPS spectra of PNCDs-5-1 (b), PNCDs-3-1 (c), and NCDs (d). (e) The P2p XPS spectrum of PNCDs-3-1. (f) The molar ratio of O/C (black) and P/C (red) in NCDs and PNCDs-m-n summarized from XPS results. (g) The percentage of C from C-O-P/C-OH groups (blue) and aromatic ring (pink) in total carbon for NCDs and PNCDs-m-n summarized from XPS results.

The Fourier transform infrared (FTIR) spectra of both PNCDs and NCDs manifested the presence of C=C, C=O, C−N, C−H, O−H, and N−H bonds (Figure 3a).[35, 39-42] Noteworthily, the distinct peaks at 1138 cm^{-1}, 928 cm^{-1}, and 618 cm^{-1} from the FTIR spectrum of PNCDs, attributing to the P−O−C, P−O, and P−C bonds, respectively,[43-46] demonstrated the successful doping of P into the NCDs, which was also verified by the X-ray photoelectron spectroscopy (XPS) results (Figure S4). The slightly increased intensity of the stretching vibration of −CH$_2$−OH (1043 cm^{-1}) and COOH (1740 cm^{-1}) in PNCDs implied that the P doping gave rise to the surface defects,[47-49] consistent with the XRD and Raman results. The C1s bands (C-O/C-P, 285.6 eV) and P2p bands (P-C at 131.7 eV and P-O at 132.5 eV) of PNCDs were detected, suggesting the formation of C−O–P and C−P (Figure 3b, 3c, 3e, and Figure S5, S6), indicative of the covalent binding of P with the framework of NCDs.[39, 50-52] It should be noted that the N1s band of PNCDs and NCDs displayed similar peaks (Figure S7), indicating that the binding information of N was not affected by P doping. As summarized in Figure 3f and 3g, PNCDs displayed a higher ratio of O/C and P/C, higher relative content of C−O–P and C−P, and lower aromatic C compared with those in NCDs (Figure 3d, S4, S5, and Table S2). Hence, the above results validated the successful synthesis of PNCDs with the formation of more surface functional groups and effective doping in the graphitic carbon framework, which altered the optical properties of the PNCDs with respect to that of NCDs (see UV-vis and PL spectra in Figure S8-S10 and more discussion in SI). It should be noted that different from NCDs, the PNCDs displayed prominent excitation-dependent properties in the whole wavelength range, which could be ascribed to different surface states introduced by P doping.
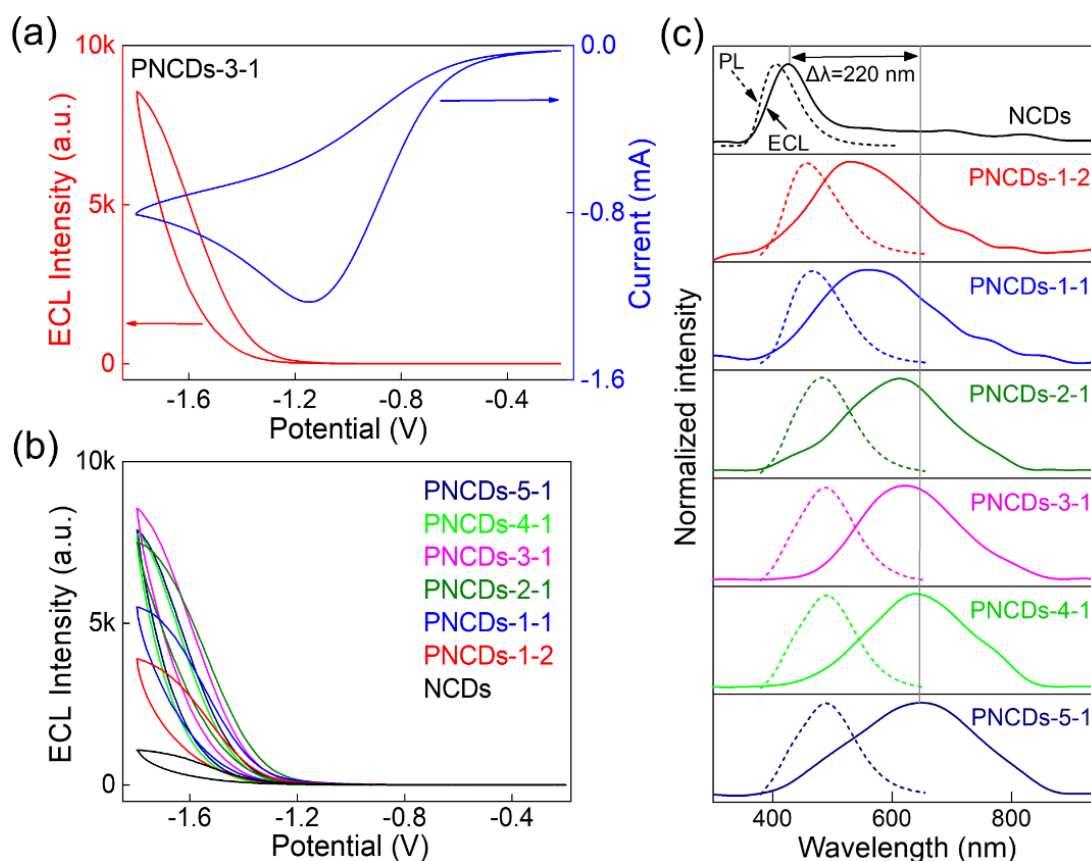
Figure 4. (a) CV (blue line) and ECL-potential (red line) curves of the PNCDs-3-1/$K_2S_2O_8$ system. (b) ECL-potential curves of NCDs and PNCDs-m-n in 0.1 M PBS (pH=7.5) containing 0.1 M $K_2S_2O_8$. Scan rate: 0.1 V/s. Concentration of NCDs and PNCDs-m-n: 0.5 mg/mL. (c) PL emission spectra (dash line) and ECL emission spectra (solid line) of NCDs and PNCDs-m-n. λ_{ex} for NCDs and PNCDs-m-n are 305 nm and 365 nm, respectively.

The unique solubility and photophysical properties make NCDs and PNCDs very promising as ECL luminophores in an aqueous solution. As annihilation-type ECL was not observed, the coreactant-type ECL was comprehensively exploited and optimized using $K_2S_2O_8$ as the coreactant (Figure S11-S14). As shown in Figure 4a and 4b, the ECL of NCDs and PNCDs onsets at about −1.2 V during the negative scan from −0.2 V to −1.8 V, following a traditional "reduction-oxidation" mechanism (Equation S2-S6). The ECL was stable and repeatable under consecutive cyclic potential scans (Figure S15), and after storage in 0.1 M PBS (pH=7.5) at 4 °C under darkness for 30 days (Figure S16). Moreover, with the increase of P dopant, both the ECL intensity (Figure 4a, 4b, and S17) and efficiency (Figure S18) increased gradually, implying the critical role of P dopant in ECL.

Table 1. Comparison of different emitters with tunable ECL emission.

Emitter	PL Emission Wavelength (nm)	ECL Wavelength (nm)	Maximum ECL Shift (nm)	Ref.
Cd-based QDs [a]	549 ~ 643	549 ~ 643	94	[15]
Ru/Ir complexes [b]	476 ~ 610	491 ~ 636	145	[13]
organic dyes [c]	445 ~ 518	450 ~ 517	67	[7]
CN-NVs [d]	446 ~ 468	450 ~ 516	66	[8]
PNCDs	405 ~ 490	425 ~ 645	220	This work

[a] CdSe/CdS/ZnS core/shell/shell QDs; [b] ruthenium(II) and iridium(III) complexes; [c] bifunctional organic dyes ; [d] graphitic carbon nitride modified with nitrogen vacancy.

For more details about the ECL emission of PNCDs, the ECL spectra at different potentials were collected. The maximum ECL emission wavelength almost kept constant when the potential varied from −1.2 V to −2.0 V (Figure S19), manifesting that there was only one single excited state corresponding to the ECL emission.[53, 54] Notably, an evident P-relevant redshift of ECL emission was observed. As shown in Figure 4c and Figure S20, the ECL spectrum of NCDs displayed a maximum emission at about 425 nm, while the PNCDs-1-2 with a small amount of P dopant showed a maximum emission at 535 nm. Increasing the P concentration resulted in a higher ECL emission wavelength, e.g., a maximum redshift of 220 nm was observed for PNCDs-5-1. It is worth noting that the facile and controllable regulation of ECL emission wavelength up to 220 nm only via a single element doping was rare (Table 1). As an example, the ECL spectra of the mixture of NCDs and PNCDs-5-1 was further collected, and dual ECL emission peaks of 425 nm and 645 nm were observed (Figure S21), ascribed to the emission of NCDs and PNCDs-5-1, respectively, displaying a great potential scheme for the wavelength-resolved ECL in the application of multicomponent analysis. In contrast, a maximum redshift of about only 85 nm for the PL emission was observed when varying the P dopant (Figure 4c and Figure S9). The comparison of ECL and PL in the dependence of redshift on the P dopants demonstrated that ECL was more sensitive to the

P doping. Moreover, the ECL emission of PNCDs-m-n with the same surface properties displayed distinct redshift up to 155 nm relative to their corresponding PL emission (Figure 4c and Figure S22, S23). The obvious difference between the ECL and PL emission highlighted the different emitting states of ECL and PL for PNCDs.
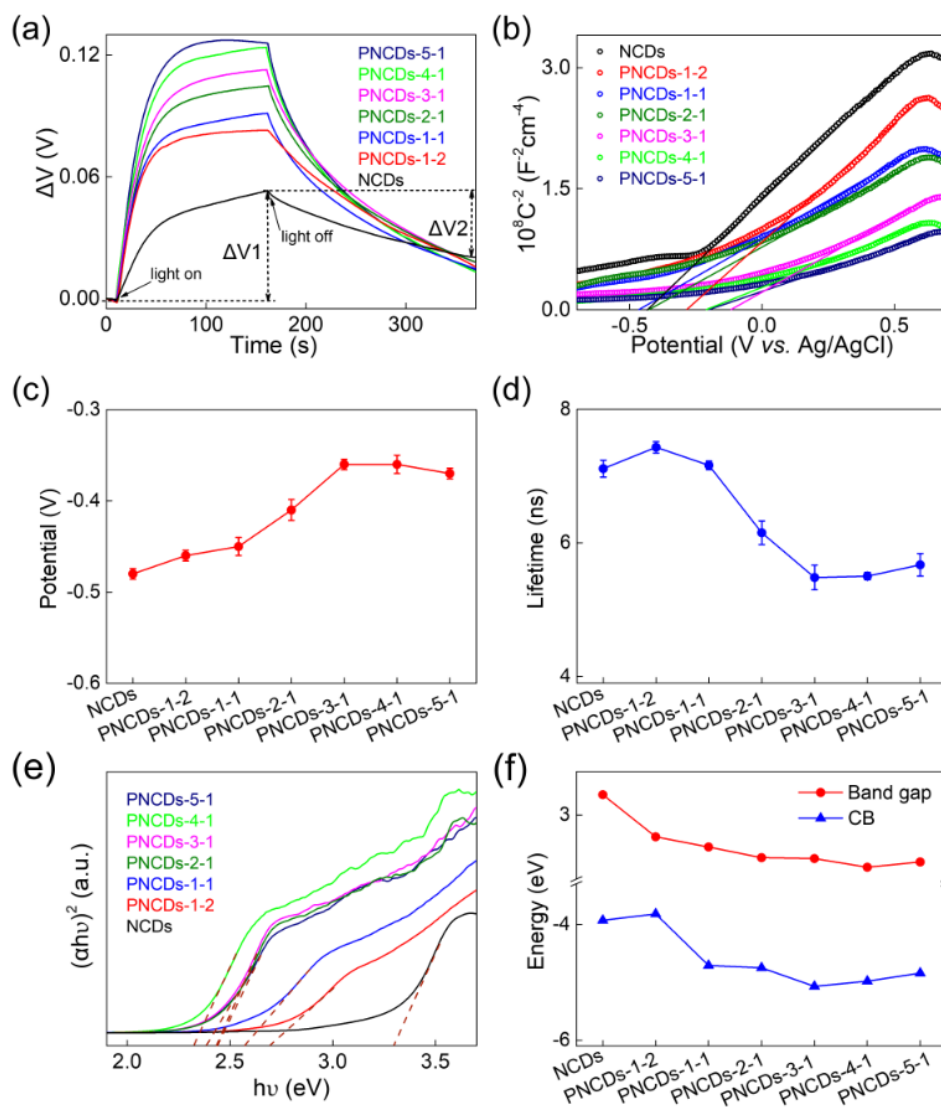

Figure 5. (a) OCP and (b) M-S plots of NCDs and PNCDs-m-n in 0.1 M KCl aqueous solution. (c) Onset reduction potentials of NCDs and PNCDs-m-n obtained from CV curves measured in the degassed PBS (0.1 M, pH = 7.5) in Figure S24. (d) PL lifetimes of NCDs and PNCDs-m-n. (e) Plots of $(\alpha h\upsilon)^2$ *vs.* photon energy and (f) energy band information of NCDs and PNCDs-m-n.

To gain more insight into the P-relevant ECL intensity and emission wavelength of PNCDs, the photoelectrochemistry was firstly explored by measuring the open circuit potential (OCP) and Mott-Schottky (M-S) plots.[55] The generation of a large OCP upon irradiation is usually considered to be a symbol of high excited electron storage ability. As shown in Figure 5a, with higher P concentration, the

10

OCP curve of PNCDs under irradiation showed a more increased ΔV_1. With the light off, the OCP of all PNCDs dropped gradually (ΔV_2). The ratio of $\Delta V_2 / \Delta V_1$ for PNCDs was closer to 1 with a higher P dopant, demonstrating less surface deep electron-trapping state. As revealed by the M-S plots (Figure 5b), PNCDs with higher P dopant had higher charge carrier density, suggesting higher electron-hole separation and electron conductivity. Thereby, both the OCP and M-S results illustrated that P doping in PNCDs could reduce the surface deep electron-trapping state, promote the electron-hole separation, and enhance the electron conductivity, all of which boosted the ECL performance of PNCDs.

The electrochemical reduction behavior of NCDs and PNCDs was further investigated in 0.1 M degassed PBS (pH=7.5) by cyclic voltammetry (CV) (Figure S24). As summarized in Figure 5c, upon increasing P dopant, the onset reduction potential gradually shifted positively from −0.48 V (for NCDs) to −0.37 V (for PNCDs-5-1), suggesting that PNCDs were more easily to be reduced than NCDs, which was one of the most critical factors for promoting ECL reactions. The facile electrochemical reduction of PNCDs could be explained by the high electron-donating property and large atom radius of the doped P atom. For additional insight into the influence of P doping on the transition processes of PNCDs, the fluorescence decay spectra of NCDs and PNCDs were measured (Figure S25). Notably, the lifetimes gradually decreased from 7.11 ns (for NCDs) to 5.67 ns (for PNCDs-5-1) with the increased P dopant (Figure 5d), indicative of an enhancement of radiative rate induced by P doping,[56] which corresponded well with the OCP and M-S results. Hence, introducing P dopant in PNCDs not only facilitated the electrochemical reduction but also promoted the photoelectrochemical processes of PNCDs, which explained well that the PNCDs with higher P dopant displayed higher ECL efficiency.

To reveal the energy band structures of PNCDs and NCDs, the UV-vis diffuse reflectance spectra (UV-vis DRS) and ultraviolet photoelectron spectroscopy (UPS) were measured. As shown in Figure 5e and Figure 5f, the band gap was achieved from the plots of $(\alpha h v)^2$ *vs.* photon energy (hv) via the transformed Kubelka−Munk function based on the UV-vis DRS analysis (Figure S26). The conduction band (CB) level of PNCDs and NCDs was further acquired based on corresponding band gap values and valence band (VB) levels from the UPS analysis (Figure S27). It was observed that the band gap became

narrower gradually, and the CB level descended progressively with the increased P dopant (Figure 5f), demonstrating that the P doping narrowed the energy band gap, which was consistent with the red-shifted PL emission of PNCDs-m-n with higher P dopant.

To get more insight into the mechanism of the effect of P doping on the ECL performance in molecular level, computational simulations were further undertaken. Three simplified structural units, a dimer of ATA for NCDs (denoted as PNCDs-0), and that of ATA with one P-containing group (designated as PNCDs-I) or two P-containing groups (defined as PNCDs-II), were proposed for NCDs and PNCDs-m-n according to above structural characterization results (Figure 6a and Figure S28). Density functional theory (DFT) calculations were carried out to assess the energy levels of the ground and excited states of these simplified structural units (Figure S29). A hole-electron composition fragments heat map was obtained from the hole-electron analysis in intrafragments (Figure 6b and Table S3, S4). Compared with PNCDs-0, the PNCDs-I in the relaxed S_1 state displayed higher hole density in the P-containing groups and higher electron density in the aromatic rings. With increasing the number of P-containing groups (for PNCDs-II), such electron and hole density change became more evident, suggesting that the electron can flow from the P-containing groups to the aromatic ring due to the significant electron-donating effect of the P dopant. Consequently, the incorporation of P dopant led to ICT in the excited state, resulting in substantial spatial separation of electron and hole distribution, which promoted the ECL process.
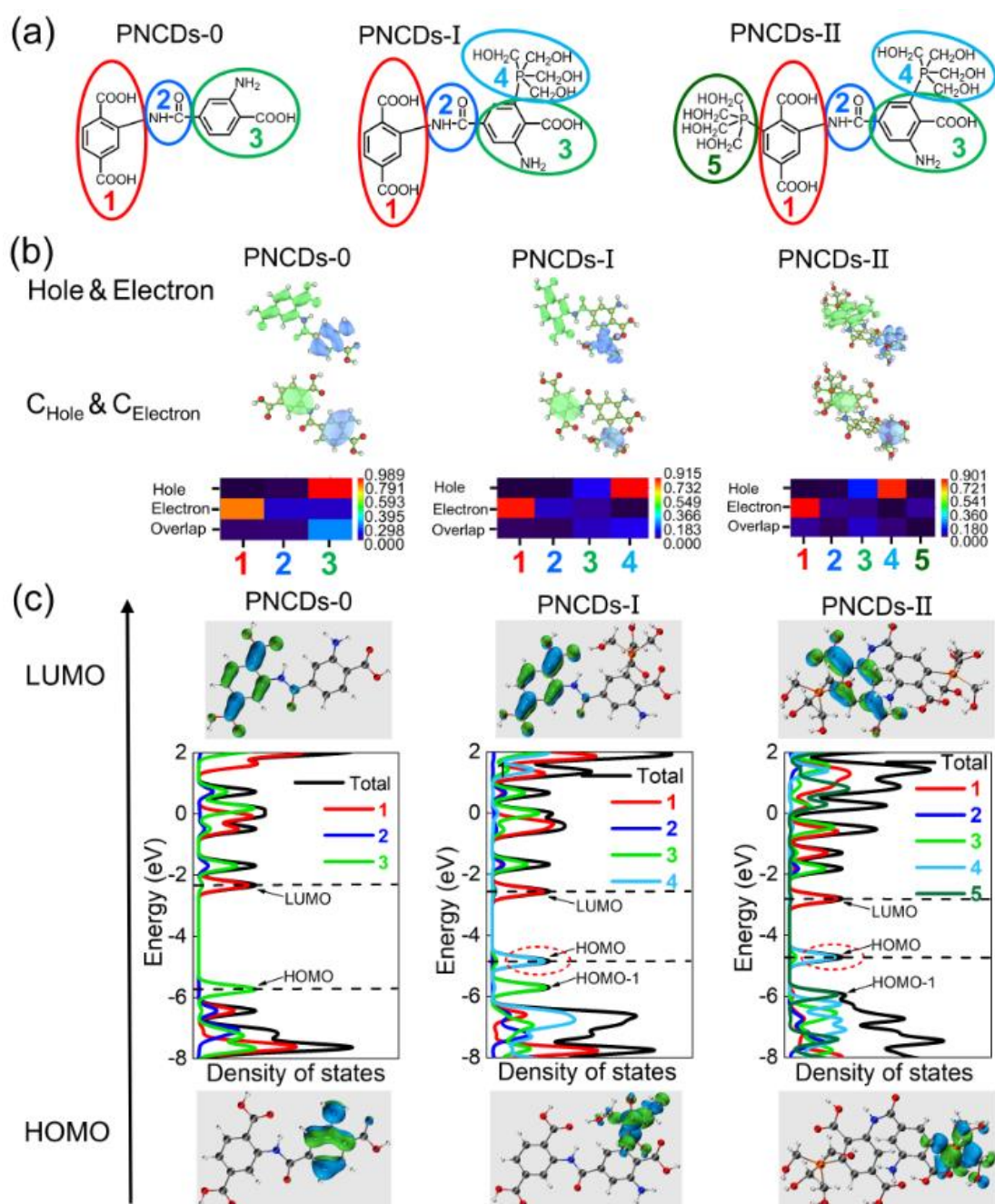
Figure 6. (a) The simplified structural units of PNCDs-0, PNCDs-I, and PNCDs-II. (b) Hole-electron analysis and hole-electron composition fragment heat map of S1 state. Green regions denote the electron distribution and blue regions denote the hole distribution. (c) The calculated molecular orbitals and density of states of the PNCDs-0, PNCDs-I, and PNCDs-II. **1**, **2**, **3**, **4**, and **5** in (b) and (c) represent the corresponding molecular fragment marked in (a).

To clarify the effect of P doping on the redshift of ECL emission, the total density of states (DOS) was also fitted by molecular orbitals, which revealed the contribution from different fragments (Figure 6c). The solid black line represents total DOS, the color lines correspond to the contribution from different fragments to DOS, and the black dash lines represent the highest occupied molecular orbital (HOMO) and lowest unoccupied molecular orbital (LUMO). In the undoped PNCDs-0 (without P doping), HOMO

and LUMO are mainly composed of fragments **3** and **1**, as indicated in Figure 6a. Compared with PNCDs-0, the energy level of LUMO in PNCDs-I decreased slightly, which may be caused by the increase of electron cloud density of the conjugated system ascribed to the P doping as discussed in the hole-electron analysis. It is worth noting that HOMO in PNCDs-I is mainly composed of the P-containing group (fragment **4**). In contrast, fragment **1,** which dominates HOMO in PNCDs-0, contributes mainly to HOMO-1 in PNCDs-I, and the energy level of HOMO-1 does not change significantly with respect to that of HOMO in PNCDs-0. Notably, the HOMO in PNCDs-I, i.e., the new orbital introduced by fragment **4** can be regarded as a new energy level generated between HOMO and LUMO of undoped PNCDs-0, which reduced the HOMO-LUMO gap from 3.40 eV to 2.28 eV (Figure S29), and further reduced the transition energy and increased the emission wavelength of ECL. In PNCDs-II, the composition of HOMO and LUMO is similar to that of PNCDs-I, except that more P dopants further narrowed the HOMO-LUMO gap to 1.92 eV and increased the emission wavelength of ECL. Thus, the incorporation of P dopants with high electron-donating ability in PNCDs not only resulted in the significant ICT effect but also led to the formation of a new energy level, narrowing the HOMO-LUMO gap, which jointly boosted the ECL performance of PNCDs. The newly generated orbital was ascribed to the surface functional groups introduced by P doping, which endowed the redshift of the ECL emission.

Conclusion

In summary, we reported the design and facile synthesis of ECL-active P-doped CDs with both tunable emission wavelength and enhanced efficiency by taking advantage of the electron-donating properties of P dopant. Varying the concentration of P dopant would lead to changes in surface functional groups and surface states, allowing fine-tuning of ECL efficiency and emission with a maximum redshift of 220 nm. In contrast, the PL emission could be tuned with a redshift of only 85 nm. The kinetics studies illustrated that the enhanced ECL performance was ascribed to the P doping-induced decrease of surface deep electron-trapping state, promoted the electron-hole separation, and enhanced the electron conductivity. Moreover, P doping regulated the energy band structures of PNCDs, e.g., the band gap was narrowed, and CB levels were progressively descended with the increased P contents. The theoretical

calculations based on a simple molecular model supported our results, which showed that the incorporation of P dopants with high electron-donating ability in CDs not only resulted in the formation of a new energy level, but also led to a significant ICT effect, which jointly boosted the ECL performance and induced the redshift of ECL emission of PNCDs. This work would provide a general and facile way to design highly efficient ECL systems with modulable emission wavelengths for various applications.

Acknowledgements

References

[1] Z. Liu, W. Qi, G. Xu, Chem. Soc. Rev., 44 (2015) 3117-3142.

[2] D. Pan, Z. Fang, E. Yang, Z. Ning, Q. Zhou, K. Chen, Y. Zheng, Y. Zhang, Y. Shen, Angew. Chem. Int. Ed., 59 (2020) 16747-16754.

[3] P. Wu, X. Hou, J.-J. Xu, H.-Y. Chen, Chem. Rev., 114 (2014) 11027-11059.

[4] L. Li, Y. Chen, J.-J. Zhu, Anal. Chem., 89 (2017) 358-371.

[5] Y. Zhao, L. Bouffier, G. Xu, G. Loget, N. Sojic, Chem. Sci., (2022).

[6] W. Miao, Chem. Rev., 108 (2008) 2506-2553.

[7] F. Rizzo, F. Polo, G. Bottaro, S. Fantacci, S. Antonello, L. Armelao, S. Quici, F. Maran, J. Am. Chem. Soc., 139 (2017) 2060-2069.

[8] R. Zou, Y. Lin, C. Lu, Anal. Chem., 93 (2021) 2678-2686.

[9] Y. Lv, Z. Zhou, Y. Shen, Q. Zhou, J. Ji, S. Liu, Y. Zhang, ACS Sens., 3 (2018) 1362-1367.

[10] J. Shu, Z. Han, T. Zheng, D. Du, G. Zou, H. Cui, Anal. Chem., 89 (2017) 12636-12640.

[11] Y.-Z. Wang, S.-Y. Ji, H.-Y. Xu, W. Zhao, J.-J. Xu, H.-Y. Chen, Anal. Chem., 90 (2018) 3570-3575.

[12] E. Kerr, E.H. Doeven, G.J. Barbante, C.F. Hogan, D.J. Bower, P.S. Donnelly, T.U. Connell, P.S. Francis, Chem. Sci., 6 (2015) 472-479.

[13] W. Guo, H. Ding, C. Gu, Y. Liu, X. Jiang, B. Su, Y. Shao, J. Am. Chem. Soc., 140 (2018) 15904-15915.

[14] S. Voci, R. Duwald, S. Grass, D.J. Hayne, L. Bouffier, P.S. Francis, J. Lacour, N. Sojic, Chem. Sci., 11 (2020) 4508-4515.

[15] Z. Cao, Y. Shu, H. Qin, B. Su, X. Peng, ACS Cent. Sci., 6 (2020) 1129-1137.

[16] M. Hesari, K.N. Swanick, J.-S. Lu, R. Whyte, S. Wang, Z. Ding, J. Am. Chem. Soc., 137 (2015) 11266-11269.

[17] J. Zhou, L. Nie, B. Zhang, G. Zou, Anal. Chem., 90 (2018) 12361-12365.

[18] Y. He, S. Hou, L. Yang, F. Zhang, G. Zou, Chem. Eur. J., 24 (2018) 9592-9597.

[19] D. Du, J. Shu, M. Guo, M.A. Haghighatbin, D. Yang, Z. Bian, H. Cui, Anal. Chem., 92 (2020) 14113-14121.

[20] J. Ge, Q. Jia, W. Liu, L. Guo, Q. Liu, M. Lan, H. Zhang, X. Meng, P. Wang, Adv. Mater., 27 (2015) 4169-4177.

[21] H. Wu, Y. Chen, X. Dai, P. Li, J.F. Stoddart, Y. Liu, J. Am. Chem. Soc., 141 (2019) 6583-6591.

[22] F. Arcudi, L. Đorđević, S. Rebeccani, M. Cacioppo, A. Zanut, G. Valenti, F. Paolucci, M. Prato, Adv. Sci., 8 (2021) 2100125.

[23] K. Jiang, X. Gao, X. Feng, Y. Wang, Z. Li, H. Lin, Angew. Chem. Int. Ed., 59 (2020) 1263-1269.

[24] S. Lu, L. Sui, J. Liu, S. Zhu, A. Chen, M. Jin, B. Yang, Adv. Mater., 29 (2017) 1603443.

[25] L. Đorđević, F. Arcudi, M. Cacioppo, M. Prato, Nat. Nanotechnol., 17 (2022) 112-130.

[26] L. Zheng, Y. Chi, Y. Dong, J. Lin, B. Wang, J. Am. Chem. Soc., 131 (2009) 4564-4565.

[27] R. Zhang, J.R. Adsetts, Y. Nie, X. Sun, Z. Ding, Carbon, 129 (2018) 45-53.

[28] X. Wang, M. Zhang, X. Huo, W. Zhao, B. Kang, J.-J. Xu, H. Chen, Nanoscale Adv., 1 (2019) 1965-1969.

[29] S. Carrara, F. Arcudi, M. Prato, L. De Cola, Angew. Chem. Int. Ed., 56 (2017) 4757-4761.

[30] S. Yang, J. Liang, S. Luo, C. Liu, Y. Tang, Anal. Chem., 85 (2013) 7720-7725.

[31] Y. Qin, N. Liu, H. Li, Y. Sun, L. Hu, S. Zhao, D. Han, Y. Liu, Z. Kang, L. Niu, J. Phys. Chem. C, 121 (2017) 27546-27554.

[32] L.-L. Li, J. Ji, R. Fei, C.-Z. Wang, Q. Lu, J.-R. Zhang, L.-P. Jiang, J.-J. Zhu, Adv. Funct. Mater., 22 (2012) 2971-2979.

[33] L. Yang, C.R. De-Jager, J.R. Adsetts, K. Chu, K. Liu, C. Zhang, Z. Ding, Anal. Chem., 93 (2021) 12409-12416.

[34] A. Chen, W. Liang, H. Wang, Y. Zhuo, Y. Chai, R. Yuan, Anal. Chem., 92 (2020) 1379-1385.

[35] H. Ding, J.-S. Wei, P. Zhang, Z.-Y. Zhou, Q.-Y. Gao, H.-M. Xiong, Small, 14 (2018) 1800612.

[36] Y.-C. Liang, S.-S. Gou, K.-K. Liu, W.-J. Wu, C.-Z. Guo, S.-Y. Lu, J.-H. Zang, X.-Y. Wu, Q. Lou, L. Dong, Y.-F. Gao, C.-X. Shan, Nano Today, 34 (2020) 100900.

[37] J. Tang, B. Kong, H. Wu, M. Xu, Y. Wang, Y. Wang, D. Zhao, G. Zheng, Adv. Mater., 25 (2013) 6569-6574.

[38] Y. Ru, L. Sui, H. Song, X. Liu, Z. Tang, S.-Q. Zang, B. Yang, S. Lu, Angew. Chem. Int. Ed., 60 (2021) 14091-14099.

[39] L. Vallan, E.P. Urriolabeitia, F. Ruipérez, J.M. Matxain, R. Canton-Vitoria, N. Tagmatarchis, A.M. Benito, W.K. Maser, J. Am. Chem. Soc., 140 (2018) 12862-12869.

[40] F. Arcudi, L. Đorđević, M. Prato, Angew. Chem. Int. Ed., 55 (2016) 2107-2112.

[41] J.-S. Wei, C. Ding, P. Zhang, H. Ding, X.-Q. Niu, Y.-Y. Ma, C. Li, Y.-G. Wang, H.-M. Xiong, Adv. Mater., 31 (2019) 1806197.

[42] C.-L. Shen, Q. Lou, J.-H. Zang, K.-K. Liu, S.-N. Qu, L. Dong, C.-X. Shan, Adv. Sci., 7 (2020) 1903525.

[43] X. Gong, Z. Li, Q. Hu, R. Zhou, S. Shuang, C. Dong, ACS Appl. Mater. Interfaces, 9 (2017) 38761-38772.

[44] Z.-Q. Xu, L.-Y. Yang, X.-Y. Fan, J.-C. Jin, J. Mei, W. Peng, F.-L. Jiang, Q. Xiao, Y. Liu, Carbon, 66 (2014) 351-360.

[45] Z. Bi, L. Huo, Q. Kong, F. Li, J. Chen, A. Ahmad, X. Wei, L. Xie, C.-M. Chen, ACS Appl. Mater. Interfaces, 11 (2019) 11421-11430.

[46] S. Bourbigot, M. Le Bras, R. Delobel, P. Bréant, J.-m. Trémillon, Carbon, 33 (1995) 283-294.

[47] H. Ding, S.-B. Yu, J.-S. Wei, H.-M. Xiong, ACS Nano, 10 (2016) 484-491.

[48] L. Bao, Z.-L. Zhang, Z.-Q. Tian, L. Zhang, C. Liu, Y. Lin, B. Qi, D.-W. Pang, Adv. Mater., 23 (2011) 5801-5806.

[49] F. Yuan, T. Yuan, L. Sui, Z. Wang, Z. Xi, Y. Li, X. Li, L. Fan, Z.a. Tan, A. Chen, M. Jin, S. Yang, Nat. Commun., 9 (2018) 2249.

[50] X. Miao, D. Qu, D. Yang, B. Nie, Y. Zhao, H. Fan, Z. Sun, Adv. Mater., 30 (2018) 1704740.

[51] C. Zhang, N. Mahmood, H. Yin, F. Liu, Y. Hou, Adv. Mater., 25 (2013) 4932-4937.

[52] K. Yuan, D. Lützenkirchen-Hecht, L. Li, L. Shuai, Y. Li, R. Cao, M. Qiu, X. Zhuang, M.K.H. Leung, Y. Chen, U. Scherf, J. Am. Chem. Soc., 142 (2020) 2404-2412.

[53] T. Zhao, Q. Zhou, Y. Lv, D. Han, K. Wu, L. Zhao, Y. Shen, S. Liu, Y. Zhang, Angew. Chem. Int. Ed., 59 (2020) 1139-1143.

[54] K. Chu, J.R. Adsetts, S. He, Z. Zhan, L. Yang, J.M. Wong, D.A. Love, Z. Ding, Chem. Eur. J., 26 (2020) 15892-15900.

[55] Y. Fang, Y. Hou, H. Yang, W. Li, J. Ma, D. Han, X. Cao, S. Liu, Y. Shen, Y. Zhang, DOI:10.26434/chemrxiv-2021-dnlsm.

[56] C.-H. Cho, C.O. Aspetti, M.E. Turk, J.M. Kikkawa, S.-W. Nam, R. Agarwal, Nat. Mater., 10 (2011) 669-675.